Distinguishing two mechanisms for enhanced ionization of H_2^+ using orthogonal two-color laser fields

Kunlong Liu [1,2,*] and Ingo Barth [2,†]

[1]*School of Physics, Huazhong University of Science and Technology, Wuhan 430074, China*
[2]*Max-Planck-Institut für Mikrostrukturphysik, Weinberg 2, 06120 Halle (Saale), Germany*

We theoretically study the ionization enhancement of the diatomic molecular ion H_2^+ at two critical internuclear distances R, using orthogonal two-color laser fields. The polarization of the fundamental infrared laser field and a weak second-harmonic field is parallel and perpendicular to the molecular axis, respectively. It is observed that adding the second-harmonic field raises slightly the first ionization peak at the smaller critical R, whereas it enhances the second one at the larger critical R significantly. We further analyze the observable evidence which distinguishes two underlying mechanisms responsible for the enhanced ionization of H_2^+: (i) the resonant excitation along with the coherent interference of the ionizing wave packets from the $1s\sigma_g$ and $2p\sigma_u$ states and (ii) the easier ionization from the up-field site of the molecule.

I. INTRODUCTION

As the simplest molecular system in nature, the hydrogen molecular ion H_2^+ has been widely applied as a prototype for studying strong-field ionization [1] and the consequential ultrafast phenomena [2] beyond atoms. While the ionization and dissociation mechanisms of H_2^+ have been extensively studied in the past decades [3,4], interest remains incessant as there are still challenges and questions raised lately by new insights [5]. In this paper, we focus on one of the intricate strong-field phenomena regarding H_2^+—its enhanced ionization (EI) at critical internuclear distances [5–28].

In the 1990s, it was reported [6–12] that, when the molecule is stretched to a critical internuclear distance R, the ionization rate increases significantly. In particular, the earliest theoretical study [6] predicted significant ionization enhancement at two critical internuclear distances of H_2^+, based on a model with fixed R. In 2015, two ionization peaks were observed in experiment using a few-cycle-pulse pump-probe technique [25]. However, the remaining question is whether there are indeed two ionization peaks at two critical internuclear distances or there is suppression of the enhancement that leads to the observation of two peaks. To answer this question, the underlying dynamics needs to be identified.

In Ref. [6], it was proposed that the ionization peaks at two internuclear distances are due to different mechanisms.

On one hand, the electron has a much higher probability of escaping directly from the upper-field-induced potential well at a critical R (typically in the range from 6 to 10 a.u.), due to the smaller ionization barrier compared to that for a hydrogen atom under the same electric field. This ionization process has been demonstrated theoretically [5,17] and in experiment [23]. On the other hand, it was shown [6] that the enhanced ionization at a relatively smaller R is related to the asymmetric electron localization on the nuclei. Strong-field-induced electron localization in dissociating H_2^+ has been studied since 2004 [29–38]. Yet, to the best of our knowledge, little direct observable evidence has been shown to associate the EI with the asymmetric electron localization except in Ref. [38]. The underlying detail of the association between EI and electron localization in H_2^+ is also unclear.

The present study aims to present and analyze the observables that distinguish two mechanisms responsible for the EI of H_2^+. To this end, we apply orthogonal two-color (OTC) laser fields to interact with H_2^+. The fundamental laser field is polarized parallel to the molecular axis and triggers the ionization. The weak second-harmonic field is polarized perpendicularly to the molecular axis and plays the role of altering the interaction. It is found that, as the pulse intensity of the second-harmonic field raises, the ionization yield at the smaller critical R (the first ionization enhancement) is hardly changed, whereas that at the larger critical R (the second ionization enhancement) is significantly increased. Further analysis suggests that such observation can be explained by two qualitatively different mechanisms responsible for the EI of H_2^+.

II. NUMERICAL METHODS

Following Ref. [6], we employ for H_2^+ the model with fixed internuclear distance R to study the dependence of the ionization dynamics on the internuclear distance. Such a

*liukunlong@hust.edu.cn
†barth@mpi-halle.mpg.de

theoretical model is justified for experiments where a few-cycle pulse is applied to probe the ionization of dissociating H_2^+ at certain internuclear distances [25]. We solve numerically the three-dimensional (3D) time-dependent Schrödinger equation (TDSE) in the Cartesian coordinate system for H_2^+. The molecule is aligned along the x axis. The fundamental infrared laser field is polarized in the x direction and the second-harmonic field is polarized in the y direction. The TDSE is given by (in atomic units)

$$i\frac{\partial}{\partial t}\Psi(\mathbf{r},t) = \left\{\frac{1}{2}[-i\nabla + \mathbf{A}(t)]^2 + V_0(\mathbf{r};R)\right\}\Psi(\mathbf{r},t), \quad (1)$$

where $V_0(\mathbf{r};R) = -(|\mathbf{r}-\mathbf{r}_+(R)|)^{-1} - (|\mathbf{r}-\mathbf{r}_-(R)|)^{-1}$ is the Coulomb potential, with $\mathbf{r}_\pm(R) = (\pm R/2, 0, 0)$. The vector potential of the few-cycle OTC pulse is given by (within the dipole approximation)

$$\mathbf{A}(t) = \sin^2\left(\frac{\pi t}{3T}\right)$$
$$\times \left[-\frac{\mathcal{E}_1}{\omega}\sin(\omega t + \phi_1)\mathbf{e}_x + \frac{\mathcal{E}_2}{2\omega}\cos(2\omega t + \phi_2)\mathbf{e}_y\right]$$
$$(2)$$

for $0 \leqslant t \leqslant 3T$, with ω, $T = 2\pi/\omega$, $\mathcal{E}_i$, and ϕ_i ($i = 1$ and 2) being the fundamental laser frequency, the optical cycle of the fundamental field, the field amplitudes, and the carrier-envelope phases (CEPs), respectively. The corresponding electric field is calculated by $\mathbf{E}(t) = -\partial\mathbf{A}(t)/\partial t$.

The TDSE is numerically solved using the split-operator spectral method [39]. The 3D grid ranges both for x and y from -107.925 to 107.925 a.u. and for z from -47.875 to 47.875 a.u. with the spacing steps of $\Delta x = \Delta y = 0.15$ a.u. and $\Delta z = 0.25$ a.u. The grid contains $1440 \times 1440 \times 384$ grid points. In our simulations, the nuclei are placed in the middle of two grid points in the x axis, in order to avoid the singularity of the Coulomb potential [40]. The time step for the evolution of the wave function is chosen as $\Delta t = 0.01$ a.u. to guarantee the numerical convergency. The initial stationary wave functions are obtained by the imaginary-time propagation method. The imaginary-time propagation is continued until the calculated ground energy is converged down to 10^{-12} in each time interval of 0.2 a.u. In real-time evolution of the wave function, the in-box and outgoing wave packets are split by an ellipsoid-shaped absorbing function, which is defined as

$$V_{\text{abs}}(x, y, z) = 1 - \left[1 + \exp\left(-\frac{r_e - r_0}{\Delta r}\right)\right]^{-1}, \quad (3)$$

with $r_e = [x^2 + (x_{\max}/y_{\max})^2 y^2 + (x_{\max}/z_{\max})^2 z^2]^{-1/2}$, where $x_{\max}$, $y_{\max}$, and $z_{\max}$ indicate the maxima of the grid in the x, y, and z dimensions, respectively. The absorber parameters are $r_0 = 100$ a.u. and $\Delta r = 3.5$ a.u., which are the ideal choice for our box size according to our tests. To avoid the unphysical reflections at boundaries of the calculation box, the absorber is applied every 40 time steps (0.4 a.u. in time). The in-box wave function is then replaced by $\Psi_{\text{new}}(t) = V_{\text{abs}}\Psi(t)$. After the laser pulse is off, the field-free propagation continues for an additional 15 fs so that the majority ionizing wave packet is absorbed. At the end of the propagation ($t = t_{\text{end}}$), the ionization yield is calculated by $Y(R, \varepsilon) = 1 - \langle\Psi(\mathbf{r}, t_{\text{end}})|\Psi(\mathbf{r}, t_{\text{end}})\rangle$ for the given R and the
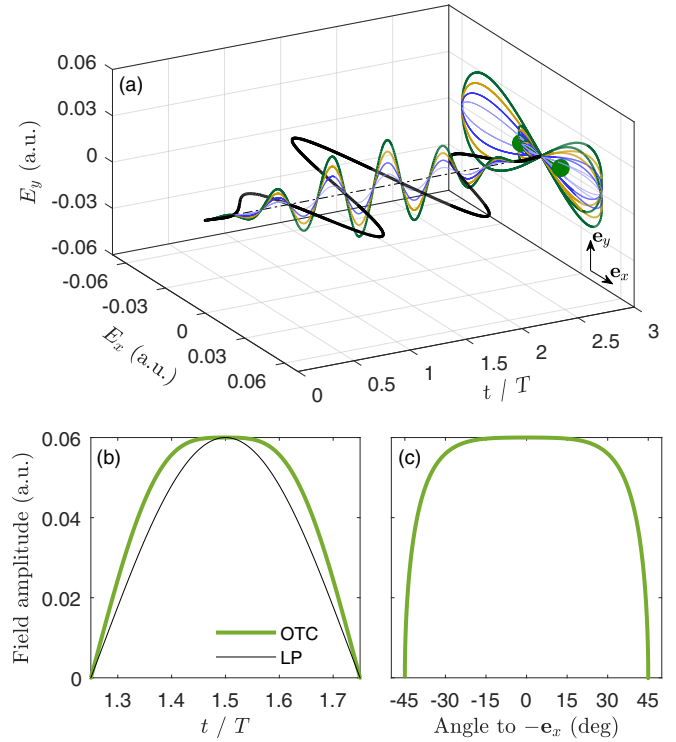

FIG. 1. (a) The OTC electric fields with $\phi_1 = \phi_2 = 0$. On its right-hand side, the curves indicate the profiles of the electric fields on the x-y plane and the solid dots show the alignment of the molecule. The 800- and 400-nm laser pulses are polarized parallel and perpendicularly to the molecular axis, respectively. (b) The instantaneous field amplitudes of the linearly polarized (LP) and OTC ($\varepsilon = 0.5$) pulses as a function of time. (c) The instantaneous field amplitude of the OTC pulse ($\varepsilon = 0.5$) within $1.25T < t < 1.75T$ versus its direction with respect to the $-\mathbf{e}_x$ direction.

field amplitude ratio $\varepsilon = \mathcal{E}_2/\mathcal{E}_1$ of the OTC field. We adopt four significant digits for the plot of the ionization yield.

III. RESULTS AND DISCUSSION

Figure 1 depicts the electric field of a three-cycle, 800-nm fundamental laser pulse with $\mathcal{E}_1 = 0.06$ a.u. and $\phi_1 = 0$ (black thick curve) and those of the orthogonal second-harmonic pulses with $\mathcal{E}_2 = \varepsilon\mathcal{E}_1$ ($\varepsilon = 1/8, 2/8, 3/8$, and $4/8$) and $\phi_2 = 0$. In this scheme, we increase the intensity of the second-harmonic field after each interaction but keep it relatively weak, in order to see how the ionization yield is altered. We have calculated the ionization yield as a function of R and ε. The results are shown in Fig. 2(a). In general, two ionization peaks are observed, in agreement with the previous study [6]. But what attracts our attention is that as the pulse intensity of the second-harmonic field increases, the first ionization peak (at $R_1 = 4.5$ a.u.) barely raises while the second ionization peak (at $R_2 = 8.1$ a.u.) is further enhanced significantly.

Before looking into the underlying mechanisms responsible for such an observation, we have checked the influence of the second-harmonic field on the ionization yield at R_1 and R_2 by varying E_2 and ϕ_2 while the fundamental pulse is unchanged. The results in Fig. 2(b) show that for both $\phi_2 = 0$ and $\phi_2 = \pi/2$ the ionization yield at R_2 is enhanced by more
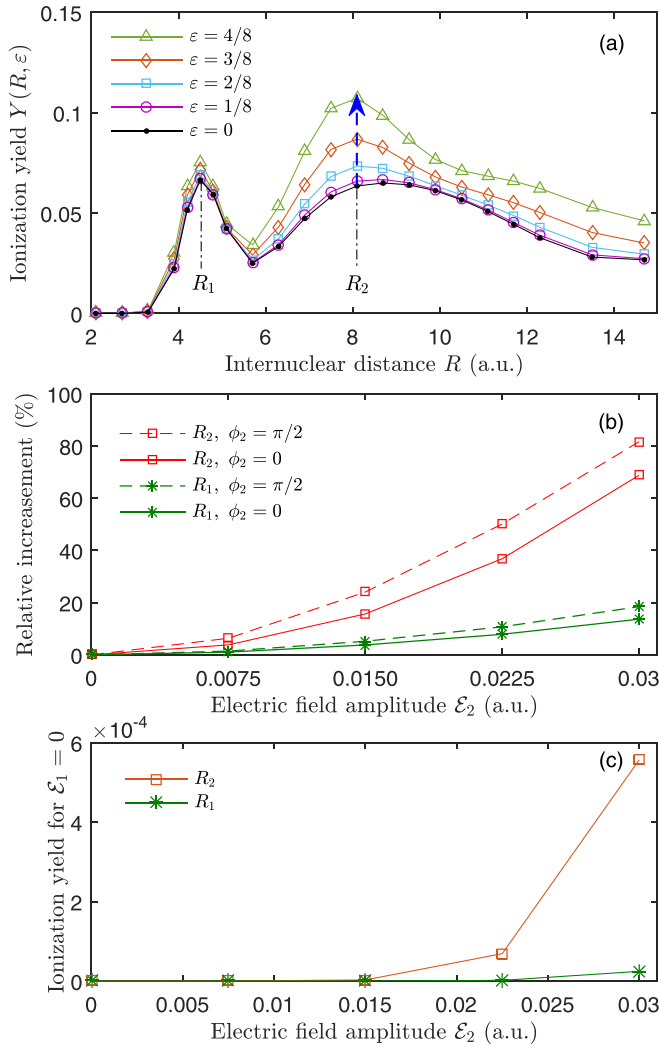
FIG. 2. (a) Ionization yield as a function of the internuclear distance R and the field amplitude ratio $\varepsilon = \mathcal{E}_2/\mathcal{E}_1$ under $\phi_1 = \phi_2 = 0$. The dashed arrow shows the further enhanced ionization with increasing ε. (b) Relative increasement of the ionization yields at R_1 and R_2 after adding the second-harmonic field with $\phi_2 = 0$ and $\phi_2 = \pi/2$, respectively. (c) Ionization yield at R_1 and R_2 by the single orthogonal second-harmonic field with $\phi_2 = 0$.

than 70% for $\mathcal{E}_2 = 0.03$ a.u., while that at R_1 is increased less than 20%. It indicates that the CEP of the second-harmonic pulse does not change essentially the distinctive tendencies of the ionization yields for R_1 and R_2 in the OTC fields, as long as the fundamental pulse remains the same. The relative enhancement of the ionization yield for $\phi_2 = \pi/2$ with respect to that for $\phi_2 = 0$ is due to the relatively larger amplitude of the OTC field at $t = 1.5T$ for $\phi_2 = \pi/2$ ($|\mathbf{E}|_{max} = \sqrt{\mathcal{E}_1^2 + \mathcal{E}_2^2}$). Note that without the fundamental pulse, the single second-harmonic field would hardly cause considerable ionization of H_2^+ at either R_1 or R_2 [see Fig. 2(c)], since it is relatively weak and is polarized perpendicularly to the molecular axis. In particular, the ionization probability is less than 0.0006 even for the strongest case as shown in Fig. 2(c), whereas the absolute ionization yield at R_2 is increased by about 0.043 (more than 70 times to 0.0006) after adding the

perpendicular pulse to the fundamental pulse. It is unlikely that the weak perpendicular component of the OTC field could independently lead to the considerably increased ionization yield at R_2 in the perpendicular direction to the molecule. This is consistent with the previous experimental observation [28] which showed that the laser pulse perpendicularly polarized with respect to the molecular axis can hardly lead to the enhanced ionization. Meanwhile, we did not find any considerable resonant excitation in the orthogonal direction by the 400-nm photons. Note that the present observation under the OTC pulses differs essentially from that in the previous study [41] where a very strong laser pulse polarized perpendicularly to the molecular axis was used. In the following, we analyze the underlying dynamics for the first ionization peak and then discuss the underlying dynamics for the second one.

First, let us revisit the explanation for two EI peaks given in the previous study [6]. As shown in Figs. 3(a) and 3(b), the energy level on the up-field site is lifted by approximately $\mathcal{E}_1 R/2$ with respect to the ground state level of H_2^+ and, as R increases, it becomes higher than the inner and outer potential barriers, eventually resulting in the enhanced ionization from the up-field site peaked at a critical R. Meanwhile, they found the significant asymmetric electron localization at a smaller critical R and believed that the enhanced population on the up-field site increases further the ionization, leading to another ionization peak. Such an explanation is certainly reasonable, and there have been studies [5,17,23] demonstrating the ionization from the up-field site of the molecules at certain internuclear distances. According to the present results shown in Fig. 2, however, the underlying dynamics for the first ionization peak could be more complicated. The reason is as follows. As shown in Fig. 1(b), the OTC field is expanded near $t = 1.5T$ with respect to the fundamental linearly polarized (LP) one. Accordingly, we depict in Fig. 1(c) the field amplitude of the OTC field as a function of its direction with respect to the $-\mathbf{e}_x$ direction. It shows that near the peak, the OTC field is still in the vicinity ($\lesssim 10°$) of the direction parallel to the molecule. Then, because the ionization rate depends exponentially on the field amplitude and the total ionization yield is the integration of the ionization rate over time, we expect, in general, more ionization yield near the peak of the OTC field with respect to the case of the LP field. In particular, near the peak of the fundamental pulse, the up-field levels at R_1 and R_2 are lifted by the fundamental field and the gaps between the lifted states and the barriers are comparable to each other for R_1 and R_2 [see Figs. 3(a) and 3(b)]. Then, if the molecule proceeds with the same mechanism (i.e., the easier ionization directly from the up-field site) at both R_1 and R_2, one would expect close relative enhancement of two ionization peaks after adding the perpendicular second-harmonic field. Especially when more population is asymmetrically localized on the up-field nucleus at R_1, the increased ionization yield at R_1 in OTC fields could have been even more pronounced if the ionization mechanism were the same for both R_1 and R_2. However, we find in contradiction that the ionization yield at R_1 is hardly increased in the OTC fields while that at R_2 is significantly increased (see Fig. 2). Therefore, the mechanism responsible for the first ionization peak should qualitatively differ from the one responsible for the second ionization peak.
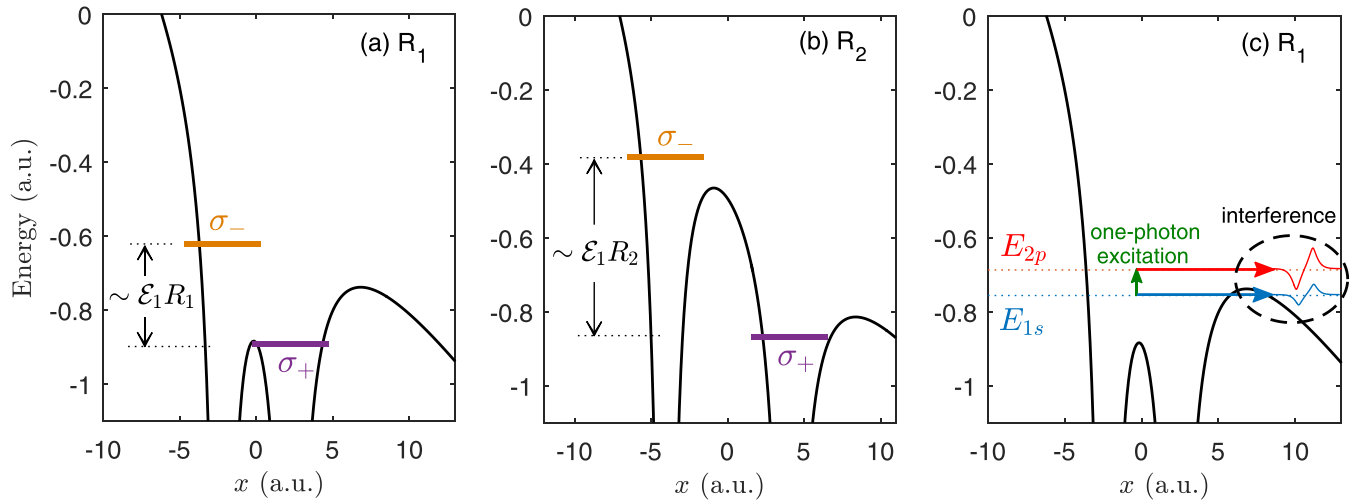
FIG. 3. The adiabatic pictures [(a) and (b)] from Ref. [6] and the diabatic picture (c) proposed in the present study to explain the enhanced ionization of H_2^+ at critical internuclear distances. The solid black curves are the laser-dressed potentials of H_2^+. In panels (a) and (b), the short thick lines are separated by $\mathcal{E}_1 R$ [4] and approximately indicate the quasistatic levels of H_2^+ in the static field. In panel (c), the horizontal dotted lines indicate the field-free energy levels of H_2^+, the arrows indicate different pathways of the ionization, and the oscillating curves inside the dashed circle are shown to illustrate the ionizing wave packets. Details are discussed in the text.

In order to reveal the underlying electronic motion during the interaction, we show in Fig. 4 the time evolutions of the electronic density distributions in the x dimension (after integrating the wave functions over the y and z dimensions) for R_1 and R_2 under the fundamental LP pulse and the OTC pulse, respectively. First of all, one can see that the second-harmonic
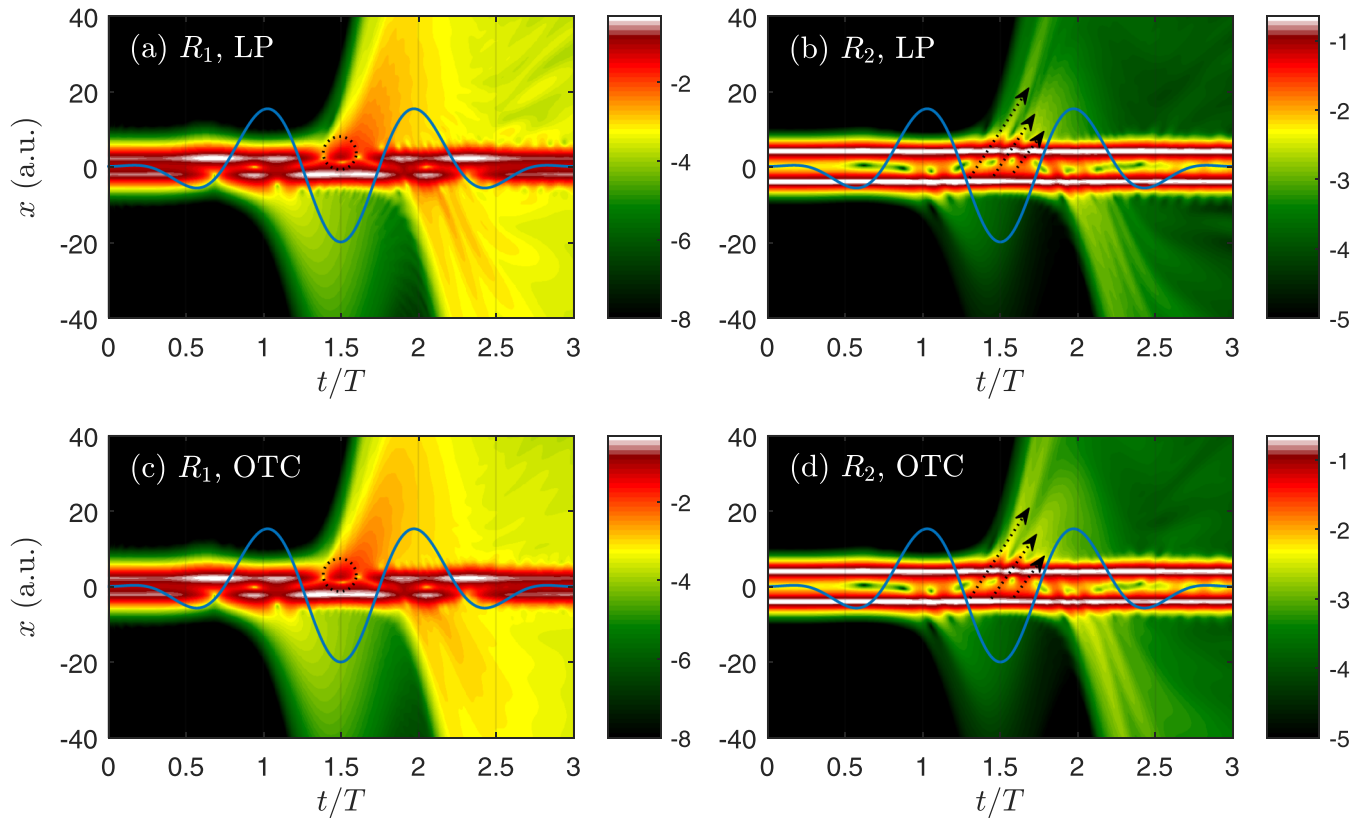

FIG. 4. Time evolutions of the electronic density distributions along the x axis. Panels (a) and (b) are for R_1 and R_2 under the LP pulse, respectively, and panels (c) and (d) are for R_1 and R_2 under the OTC pulse ($\varepsilon = 0.5$ and $\phi_1 = \phi_2 = 0$), respectively. The color plots are in logarithmic scale. The solid curves indicate the electric field profile of the fundamental LP pulse. The dotted circles in panels (a) and (c) outline the temporary localization of the electronic density on the down-field site. The dotted arrows in panels (b) and (d) outline the pathways of the wave packets ionizing from the up-field site.
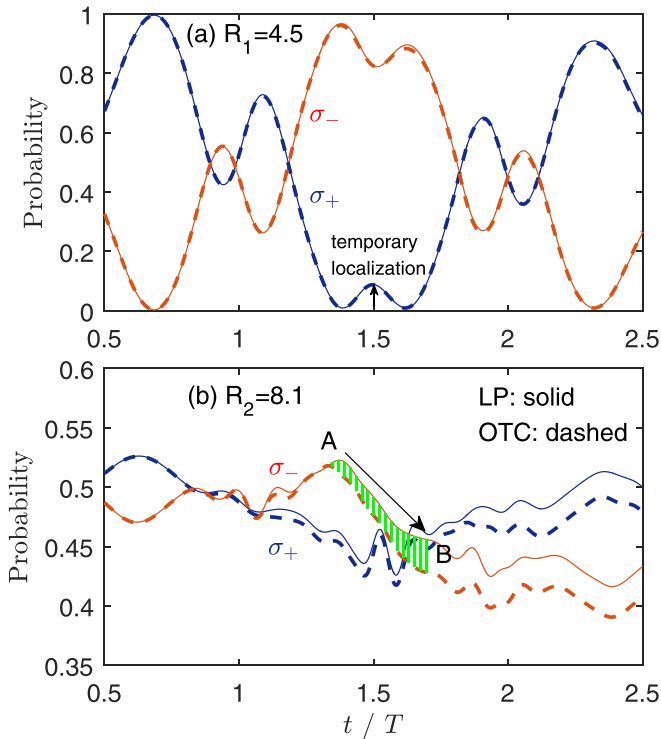
FIG. 5. Time evolutions of the probabilities of the $\sigma_\pm$ states in the LP (solid) and OTC (dashed) fields for R_1 (a) and R_2 (b). The laser parameters are the same as those in Fig. 4. The arrow pointing from A to B in panel (b) shows the continuously decreasing tendency of the up-field population (σ_-) near $t = 1.5T$ for both LP and OTC pulses. The vertical-line shadow in panel (b) indicates the additional depletion of the up-field population in the OTC field with respect to that in the LP field near the field maximum.

field hardly modifies the evolution of the bound density in the x dimension, while it slightly modifies the interference pattern of ionizing wave packets. Second, it is noticeable that for R_1 the electron density is localized on the up-field nucleus ($x = -R_1/2$) around the field maximum, which is in agreement with the previous study [6]. It indicates that the first ionization peak is somehow associated with the asymmetric electron localization, which will be explained later.

For a deeper insight, we define the wave functions $\Psi_{\sigma_\pm} = (\Psi_{1s\sigma_g} \pm \Psi_{2p\sigma_u})/2$ to represent the temporary states in which the wave packet is localized on the left (σ_-) and right (σ_+) nucleus, respectively, with $\Psi_{1s\sigma_g}$ and $\Psi_{2p\sigma_u}$ being the stationary wave functions of the ground and first excited states. We have calculated the time-dependent population of $\sigma_\pm$ by $Y_{\sigma_\pm}(t) = |\langle\Psi_{\sigma_\pm}|\Psi(t)\rangle|^2$. The results are shown in Fig. 5, where the solid and dashed curves represent the cases using the LP and OTC pulses, respectively. In Fig. 5(a), for R_1, it is shown that before the electric field hits the maximum ($t = 1.5T$) the population is mostly on the up-field site (σ_-), creating a hole on the down-field site. Then, the population on the up-field site starts decreasing and, meanwhile, the temporary population appears on the down-field site (σ_+). Such a feature can also be seen in Figs. 4(a) and 4(c), where the dotted circles outline the temporary localization of the electron on the down-field site. Therefore, it is most likely that the ionizing electron originates

from the up-field site, but instead of escaping directly from the up-field site, it has a certain probability to recombine with the down-field hole and then proceeds to a tunneling ionization from the down-field site. For R_1, the tunneling from the down-field site has been confirmed by the Gaussian distribution of the lateral photoelectron momentum in our previous study [17].

At R_1, the ionization is taking place while the population is being intertransferred between the $\sigma_\pm$ states at the same time due to the resonant coupling. It is therefore difficult to exactly tell from Fig. 5(a) whether the depletion of a given state (σ_+ or σ_-) is due to the ionization or due to the population transfer to the other state. Here, we seek from an alternative perspective for the explanation of the striking ionization enhancement at R_1. The physical picture is shown in Fig. 3(c). First of all, instead of considering the left and right sites of the molecule, we treat it as one whole system since the ground state level E_{1s} is higher than the inner barrier. According to the R-dependent energy levels of H_2^+, the one-photon (800 nm) crossing between $1s\sigma_g$ and $2p\sigma_u$ is at $R = 4.8$ a.u. So, in this diabatic picture, the first excited state is populated during the interaction via the one-photon resonant excitation near the crossing. Then, the excited system is ready to be ionized much more easily, which is the prerequisite for the enhanced ionization near R_1. Meanwhile, the ground state of H_2^+ at R_1 has also certain probability to be ionized due to the thin laser-dressed barrier [see Fig. 3(c)]. In this picture, one can consider that the fundamental field is the superposition of two pulses with the same wavelength, which play different roles during the interaction. One is to trigger the resonant excitation and the other is to drive the ionization by bending the Coulomb potential. Once the ground and first excited states are populated, there is the possibility for the ionization from either state in the external field and the ionizing wave packets from two states will interfere with each other. Eventually, from the viewpoint of energy reservation, the ionizing wave packet having absorbed N photons from the ground state and that having absorbed $N - 1$ photons from the first excited state share the same kinetic energy and thus coherently interfere in continuum. Depending on the phase difference, the constructive or destructive interference will *enhance* or *reduce* the ionization, respectively. Note that because of the band width of the laser pulse, the physical picture discussed here is still justified when R is around the one-photon crossing and when Stark shifts of the energy levels are taken into account. In short, we propose that the first ionization peak near the one-photon crossing is determined by the resonant excitation *and* the coherent interference of the ionizing wave packets from the $1s\sigma_g$ and $2p\sigma_u$ states.

The results further supporting our explanation of the underlying mechanism can be found in Fig. 6. On one hand, by varying the CEP of the few-cycle pulse, the interference process is modified and we indeed observe in Fig. 6(a) that the first peak is altered gradually when the CEP is changed. On the other hand, we compare in Fig. 6(b) the ionization yields for the 800- and 1200-nm pulses with otherwise the same parameters. The peak for the 1200-nm pulse is observed at a larger internuclear distance, as the resonant excitation for the 1200-nm photon is at $R = 5.3$ a.u. Besides, the underlying dynamics can also be modified by the intensity [31,32], the
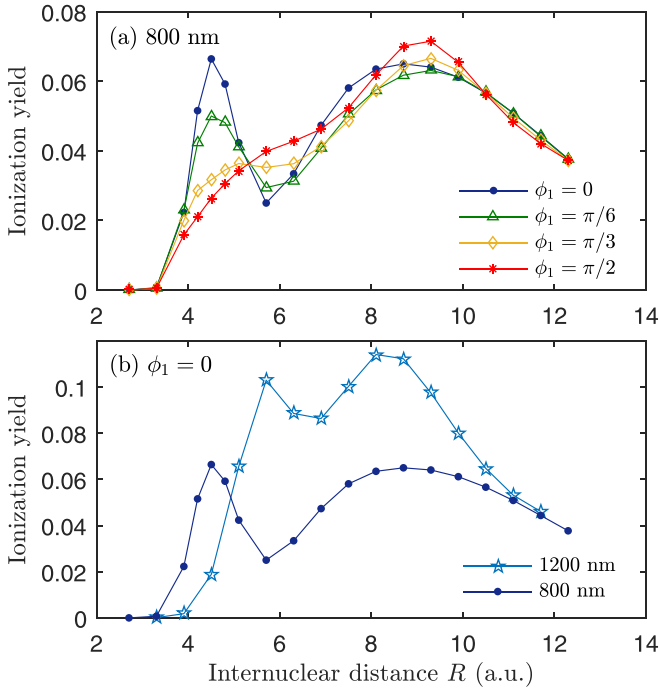
FIG. 6. Ionization yield as a function of the internuclear distance R under the fundamental LP pulses: (a) for the 800-nm pulses with different CEPs and (b) for the fixed CEP ($\phi_1 = 0$) but two different wavelengths.

FIG. 7. The x-component electric field (upper panel) and the time-dependent depletion difference (dashed curves) between the LP and OTC cases [i.e., the difference between the solid and dashed curves shown in Fig. 5(b)] for the σ_+ and σ_- states, respectively. The solid curves in the lower panel are the average of the depletion difference over a range of ± 12 a.u. in time at each time step. The texts in the boxes indicate the states that are on the up-field site near the field extrema. The solid and dotted arrows show the tendencies of the depletion difference for the up- and down-field sites, respectively.

wavelength [35,36], or even the pulse duration [33] of the fundamental LP pulse, leading to the modification of the first ionization enhancement under different laser parameters. This explains that among the previous studies [7,10,15–18], the first ionization peak is observed at different R but it is always near the one-photon crossing. On the other hand, in the present study the second-harmonic electric field perpendicular to the molecular axis does not contribute to the coupling between $1s\sigma_g$ and $2p\sigma_u$ and, thus, it hardly affects the phase shifts between the ionizing wave packets from these two states. Only the transverse drifts of the ionizing wave packets in the OTC fields cause small modification of their interference, as shown in Figs. 4(a) and 4(c). Therefore, it explains the observation in Fig. 2 that, with a fixed fundamental pulse, the first ionization peak is hardly changed by adding the perpendicular second-harmonic field. Furthermore, according to the results shown in Fig. 6(a), we expect that the CEP-averaged R-dependent ionization yields under the fundamental LP pulse would still exhibit the double-peak structure, though the locations of the ionization peaks differ from those shown in the previous studies [25,41] due to the laser parameters being chosen differently.

In addition, we can now understand the association of the asymmetric electron localization with the first ionization peak. The electron localization results from the superposition of the ground and first excited states, and the asymmetry depends on the relative phase shift between these two states. Meanwhile, the first ionization peak also relies on the phase shifts of the ionizing wave packets from these two states. As a result, when the first excited state is resonantly populated at R_1, the enhanced ionization and the asymmetric electron localization
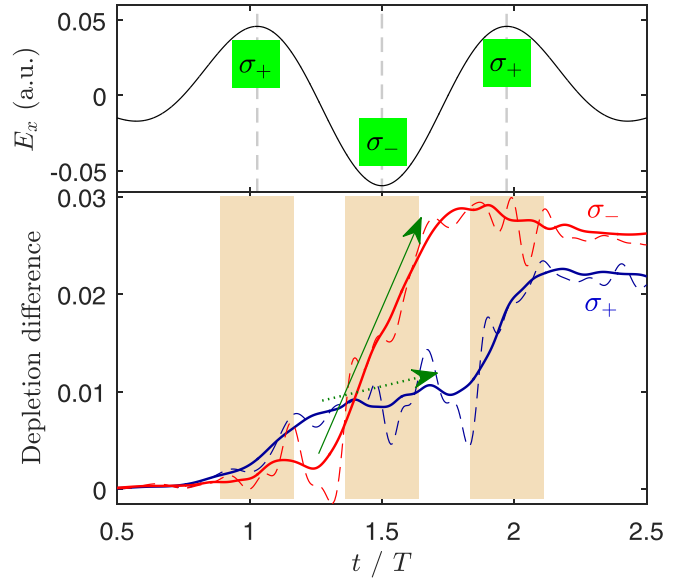
would take place at the same time under the same phase shift between the ground and first excited states. This finding agrees well with the previous observation that the enhanced ionization is always associated with the electron localization [6].

Finally, we turn to the underlying dynamics for the second ionization peak, which has been well demonstrated in the previous studies [5,6,17,23]. At R_2, two nuclei are well separated by the inner barrier. As shown in Fig. 3(b) and discussed previously, the energy level on the up-field site is lifted and, thus, the overbarrier ionization from the up-field site leads to the enhanced ionization at R_2. From Figs. 4(b) and 4(d), we indeed observe roughly the transportation of the population from the up-field site to the continuum, as indicated by the dotted arrows. We can also see from the color scale that the ionizing wave packet is enhanced in the OTC field [Fig. 4(d)] with respect to that in the LP field [Fig. 4(b)]. In order to confirm where the additional ionizing population comes from in the case of OTC fields, we have calculated the evolutions of the population of $\sigma_\pm$ at R_2 for the OTC and LP pulses and show them in Fig. 5(b). Because of the relatively larger internuclear distance at R_2, the asymmetric electron localization is suppressed. Thus, from the straight depletion of the population of σ_- near $t = 1.5T$, as indicated by the arrow in Fig. 5(b), we can generally tell that for both OTC and LP pulses the ionization from the up-field site is more pronounced than that from the down-field site. Meanwhile, as indicated by the vertical-line shadow, the population of σ_- (up-field site) in the OTC field is additionally depleted with respect to that in the LP field.

For a deeper insight into the enhanced ionization at R_2 after adding the orthogonal second-harmonic field, we show in Fig. 7 the time-dependent depletion differences between the LP and OTC cases [i.e., the difference between the solid and dashed curves shown in Fig. 5(b)] for the σ_+ and σ_- states, respectively, along with the fundamental electric field. As shown by the solid arrow, the depletion difference for σ_- increases significantly near $t = 1.5T$, indicating that the up-field population is much more depleted after adding the orthogonal field. In contrast, as shown by the dotted arrow, the depletion difference for the down-field state (i.e., σ_+) grows slower, indicating that the down-field population is also further depleted after adding the orthogonal field, but the increased depletion is not as significant as that of the up-field site. Note that the faster depletion of the up-field population can also be observed at the other two local peaks of the electric field where σ_+ is on the up-field site, as shown in Fig. 7. The results suggest that the ionization yield from the up-field site at R_2 is further enhanced when the intensity of the second-harmonic field is increased, supporting the mechanism of easier ionization from the up-field site of the molecule.

IV. CONCLUSION

In conclusion, we have theoretically studied the enhanced ionization of H_2^+ using the OTC fields. The results have shown the distinctive patterns of the ionization at two critical internuclear distances, which can be considered as the observable evidence demonstrating two qualitatively different underlying mechanisms for the enhanced ionization. In particular, we propose that the ionization peak near the one-photon crossing can be explained by the resonant excitation along with the coherent interference of the ionizing wave packets from the $1s\sigma_g$ and $2p\sigma_u$ states. Also, we confirm that the ionization enhancement at the larger critical internuclear distance is due to the easier ionization from the up-field site of the molecule.

[1] M. Y. Ivanov, M. Spanner, and O. Smirnova, J. Mod. Opt. **52**, 165 (2005).

[2] F. Krausz and M. Ivanov, Rev. Mod. Phys. **81**, 163 (2009).

[3] J. H. Posthumus, Rep. Prog. Phys. **67**, 623 (2004).

[4] H. Ibrahim *et al.*, J. Phys. B: At., Mol. Opt. Phys. **51**, 042002 (2018).

[5] H. Chomet, D. Sarkar, and C. Figueira de Morisson Faria, New J. Phys. **21**, 123004 (2019).

[6] T. Zuo and A. D. Bandrauk, Phys. Rev. A **52**, R2511(R) (1995).

[7] J. H. Posthumus *et al.*, J. Phys. B: At., Mol. Opt. Phys. **28**, L349 (1995).

[8] S. Chelkowski and A. D. Bandrauk, J. Phys. B **28**, L723 (1995).

[9] T. Seideman, M. Y. Ivanov, and P. B. Corkum, Phys. Rev. Lett. **75**, 2819 (1995).

[10] Z. Mulyukov, M. Pont, and R. Shakeshaft, Phys. Rev. A **54**, 4299 (1996).

[11] E. Constant, H. Stapelfeldt, and P. B. Corkum, Phys. Rev. Lett. **76**, 4140 (1996).

[12] D. Normand and M. Schmidt, Phys. Rev. A **53**, R1958(R) (1996).

[13] M. J. DeWitt and R. J. Levis, J. Chem. Phys. **108**, 7045 (1998).

[14] A. D. Bandrauk and J. Ruel, Phys. Rev. A **59**, 2153 (1999).

[15] X. Chu and S.-I. Chu, Phys. Rev. A **63**, 013414 (2000).

[16] L. Xin, H.-C. Qin, W.-Y. Wu, and F. He, Phys. Rev. A **92**, 063803 (2015).

[17] K. Liu and I. Barth, Phys. Rev. Lett. **119**, 243204 (2017).

[18] H. Liang *et al.*, J. Phys. B: At., Mol. Opt. Phys. **50**, 174002 (2017).

[19] D. Pavičič, A. Kiess, T. W. Hänsch, and H. Figger, Phys. Rev. Lett. **94**, 163002 (2005).

[20] N. Suzuki, I. Kawata, and K. Yamashita, Chem. Phys. **338**, 348 (2007).

[21] N. Takemoto and A. Becker, Phys. Rev. Lett. **105**, 203004 (2010).

[22] I. Bocharova *et al.*, Phys. Rev. Lett. **107**, 063201 (2011).

[23] J. Wu, M. Meckel, L. Ph. H. Schmidt, M. Kunitski, S. Voss, H. Sann, H. Kim, T. Jahnke, A. Czasch, and R. Dörner, Nat. Commun. **3**, 1113 (2012).

[24] H. Chen, V. Tagliamonti, and G. N. Gibson, Phys. Rev. A **86**, 051403(R) (2012).

[25] H. Xu, F. He, D. Kielpinski, R. T. Sang, and I. V. Litvinyuk, Sci. Rep. **5**, 13527 (2015).

[26] S. Erattupuzha *et al.*, J. Phys. B: At., Mol. Opt. Phys. **50**, 125601 (2017).

[27] M. Paul and S. Gräfe, Phys. Rev. A **99**, 053414 (2019).

[28] W. Lai and C. Guo, Phys. Rev. A **93**, 043401 (2016).

[29] V. Roudnev, B. D. Esry, and I. Ben-Itzhak, Phys. Rev. Lett. **93**, 163601 (2004).

[30] M. F. Kling *et al.*, Science **312**, 246 (2006).

[31] F. He, C. Ruiz, and A. Becker, Phys. Rev. Lett. **99**, 083002 (2007).

[32] F. He, A. Becker, and U. Thumm, Phys. Rev. Lett. **101**, 213002 (2008).

[33] P. Lan, E. J. Takahashi, and K. Midorikawa, Phys. Rev. A **86**, 013418 (2012).

[34] G. Sansone *et al.*, Nature (London) **465**, 763 (2010).

[35] K. Liu, W. Hong, Q. Zhang, and P. Lu, Opt. Express **19**, 26359 (2011).

[36] K. Liu, Q. Zhang, P. Lan, and P. Lu, Opt. Express **21**, 5107 (2013).

[37] Z. Wang *et al.*, J. Phys. B: At., Mol. Opt. Phys. **48**, 015601 (2015).

[38] H. Xu *et al.*, Nat. Commun. **8**, 15849 (2017).

[39] M. D. Feit, J. A. Fleck, Jr., and A. Steiger, J. Comput. Phys. **47**, 412 (1982).

[40] Y. Fu, J. Zeng, and J. Yuan, Comput. Phys. Commun. **210**, 181 (2017).

[41] A. D. Bandrauk and K.-J. Yuan, J. Phys. B: At., Mol. Opt. Phys. **51**, 074001 (2018).